J Solid State Electrochem (2010) 14:289–303
DOI 10.1007/s10008-009-0811-8

ORIGINAL PAPER

Redox-active silica nanoparticles. Part 4. Synthesis, size distribution, and electrochemical adsorption behavior of ferrocene- and (diamine)(diphosphine)-ruthenium(II)-modified Stöber silica colloidal particles

Filip Novak · Nicolas Plumeré · Bernd Schetter · Bernd Speiser · Diana Straub · Hermann A. Mayer · Michaela Reginek · Klaus Albert · Gerd Fischer · Christoph Meyer · Hans-Joachim Egelhaaf · Børre Børresen

Received: 31 December 2008 / Revised: 17 February 2009 / Accepted: 18 February 2009 / Published online: 14 March 2009

Abstract Stöber silica nanoparticles with a diameter of approximately 800 nm are covalently modified by redox-active ferrocene or (diamine)(diphosphine) ruthenium(II) units attached to a spacer. The particles are characterized by NMR spectroscopic and chemical techniques. Two variants of modification by condensation are compared. Besides an estimation of the size and the particle porosity, the agglomeration behavior in solvents of different polarity is investigated. The adsorption of the particles to an electrode surface is followed.

Keywords Stöber process · Silica nanoparticles · Redox modification · Adsorption

Part 3: see, ref. [1]

F. Novak · N. Plumeré · B. Schetter · B. Speiser (✉) · D. Straub · K. Albert · G. Fischer · C. Meyer
Institut für Organische Chemie, Universität Tübingen, Auf der Morgenstelle 18, 72076 Tübingen, Germany
e-mail: bernd.speiser@uni-tuebingen.de

H. A. Mayer · M. Reginek
Institut für Anorganische Chemie, Universität Tübingen, Auf der Morgenstelle 18, 72076 Tübingen, Germany

H.-J. Egelhaaf
Institut für Physikalische und Theoretische Chemie, Universität Tübingen, Auf der Morgenstelle 8, 72076 Tübingen, Germany

B. Børresen
Institutt for materialteknologi, NTNU, Sem Sælands vei 6, 7491 Trondheim, Norway

Introduction

Small, submicroscopic structures such as particles of nanometric sizes or dendrimers have attracted much scientific interest [2–13]. Objects in the "meso" world between the molecular and continuous domains [11] often exhibit properties that cannot be directly deduced from the bulk material's behavior. Applications in catalysis [4, 6], energy storage and conversion [14, 15], life sciences [2, 16–18], and many more have been discussed.

In order to tailor such nanoparticles to specific needs, they were modified by using them as scaffolds [5] for molecular reactions. Covering particles with polymeric materials (core-shell structures [19]) also provided a high variability of properties.

In particular, various types of nano-objects (see, e.g., [14, 18, 19]) were based on silica preparations. While aerogels exhibit high surface areas due to their porous structure [15], other silica materials are characterized by low porosity. Among the latter, the spherical, nonporous, and highly monodisperse [20] Stöber silica particles [21] could provide a unique support for covalently bound molecular modifiers. Their structure and symmetry ensures a high homogeneity of all surface-attached molecules in terms of environment, bonding, and accessibility. Furthermore, their size (between 50 nm and roughly 10 μm [20] depending on synthetic conditions) would allow simple separation from reaction mixtures. Thus, modified Stöber particles are inorganic–organic hybrid materials and could form the basis for regenerable catalysts, similar

to those suggested in the "chemistry in interphases" context [22].

Recently [23], we reported the synthesis and preliminary characterization of redox-actively modified Stöber silica particles, including those with catalytic properties. Shortly after (in terms of final version date) ours, similar materials were described by another group [24]. In the present paper, we discuss in more detail experiments to characterize some of our preparations.

It is a first objective of this paper to show that our base material generated by the Stöber process (diameter $d \approx 800$ nm; material **M0**) meets the size distribution and porosity requirements needed for reproducible work with modified particles in the context presented above.

The presence of silanol groups on the silica particle surface [25] then provides one opportunity for covalent attachment of redox and/or catalytically active species. The present work will characterize particles modified with ferrocene (fc, **1**), and a ruthenium complex moiety **2** by spectroscopic and physicochemical methods. Fc is regarded as a simple model example of a one-electron redox system that is relatively stable in two oxidation states. Ruthenium(II) complexes with a diamino and a diphosphine ligand prove (apart from exhibiting redox activity [26, 27]) to be efficient catalysts for the hydrogenation of C=C and C=O double bonds [28–32] in a way similar to Noyori's catalyst [33, 34].

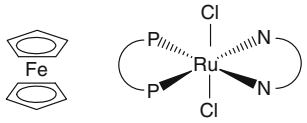

1 **2**

Covalent surface modification of Stöber silica nanoparticles with a redox-active molecule XY could be achieved by two pathways (Scheme 1): In route I, a trialkoxysilane-substituted linker L with a reactive end group X is condensed to the silica surface, and X reacts with Y in a second step. Route I mimics the concept of a stepwise "solid phase synthesis" [35]. On the other hand, Y could be bound to L first in a homogeneous reaction, and the resulting conjugate would then be attached to the silica particles by condensation (route II). These two routes will be compared in the present work for the attachment of **1** and **2** (Scheme 2). While route I proceeds through aminoalkyl modified silica particles **M1** and **M2**, which react with ferrocene carboxylic acid **4** or the precursor complex **5** in an amide bond formation or a ligand exchange reaction, respectively, route II requires prior synthesis and isolation of conjugates **3** or **6**, which are directly bonded to the bare particles **M0**. Note that we do not specify all bonds at the linker Si atoms in **M3** and **M4**. It is known that various bonding patterns of a (trialkoxy)silane to a SiO_2 surface may be formed (for the case of porous silica, see [36]).

Finally, the redox activity of the attached species opens the possibility of electrochemical characterization by means of, in particular, cyclic voltammetry (CV) and electrochemical quartz crystal nanobalance (EQCN) gravimetry. The importance of functionalized organic–silica hybrid materials in electrochemistry has recently been emphasized [37]. In our context, electrochemical activation and switching of catalysts immobilized on an electrode surface [38] present additional opportunities. The mobility of the surface-bound redox-active centers is then crucial for any catalytic application since the kinetics of the overall catalytic process is governed by this factor [39]. Studies on dendrimers [40–44] have emphasized the importance of the diffusional behavior within the redox-active shell as regards electron communication between the electrode and the active centers. Materials **M3** and **M4** show similar behavior [23], while the catalytic properties of a ruthenium hydrogenation catalyst remain intact in **M4**. As an extension, a characterization of the adsorption processes of **M3** and **M4** on Pt electrodes is a fourth objective of the present work.

Experimental section

Solvents and electrolytes

Toluene was refluxed over Na in the presence of benzophenone (both Fluka, Switzerland) until the solution turned blue before distillation. Acetonitrile was

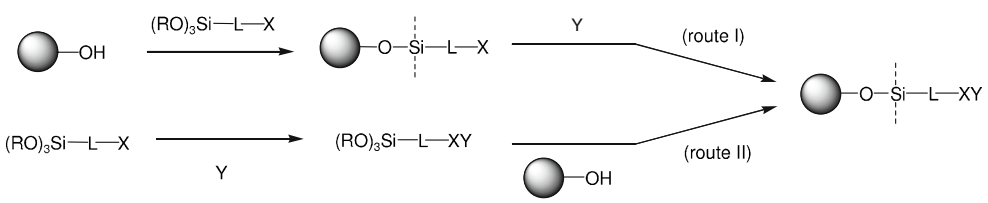

Scheme 1 Modification pathways of Stöber silica nanoparticles used in this work

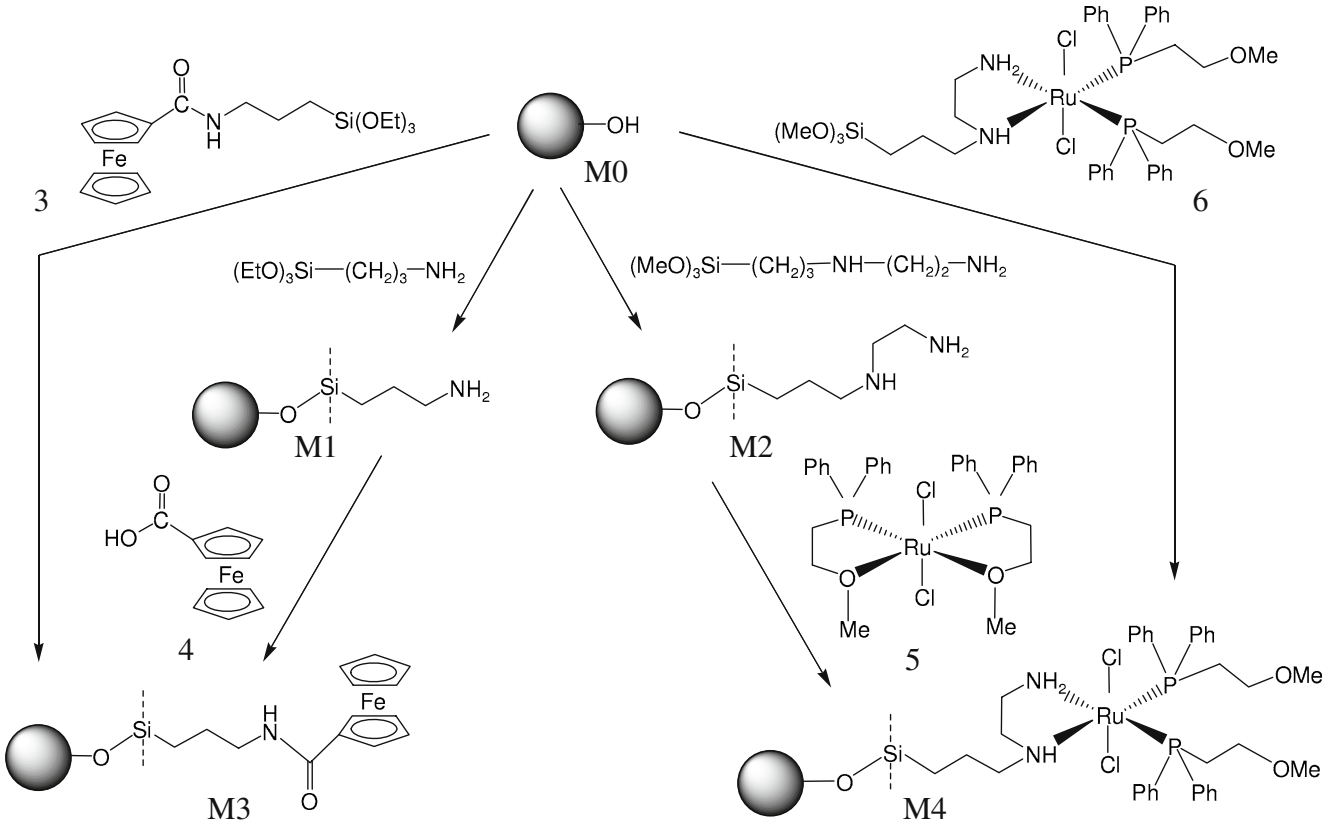

Scheme 2 Synthesis of redox-actively modified Stöber silica particles

distilled from P_2O_5 (Aldrich, USA) and, subsequently, NaH (Fluka). Dichloromethane was distilled without a drying agent. All distillations were performed under Ar. For electrochemical purposes, dichloromethane and acetonitrile were further dried by standing for 10–12 h over activated Al_2O_3 [45].

For the cyclic voltammetric investigations, dichloromethane and acetonitrile were used as the solvents with tetra-*n*-butylammonium hexafluorophosphate (NBu_4PF_6 [46]) as the supporting electrolyte (0.1 M). The electrolyte dichloromethane + NBu_4PF_6 was degassed by three freeze-pump-thaw cycles before transferring it into the electrochemical cell under argon, while acetonitrile + NBu_4PF_6 was degassed by bubbling with Ar (overpressure 0.6 atm) for 30 min.

Physicochemical methods

Scanning electron microscopy

Field emission scanning electron microscope (FESEM) images of **M0** were obtained at the *Institut für Physik* (*Universität Tübingen*, Germany) on an XL 30 Microscope (Philips, Netherlands) after immobilization on a Pt sheet electrode and Au sputtering. FESEM imaging of **M3** and **M4** was performed on a S-4300 SE/N microscope (Hitachi, USA) controlled by a standard program from Hitachi. The initial energy of the electron beam was adjusted to 5 keV. The Pt-foils for the immobilization of **M3** and **M4** were polished with carbon disks (Praktal, Norway) in decreasing grain sizes of 4, 2, 1, 0.5, and 0.05 μm. After immobilization from a CH_3CN suspension of the particles ($c = 5$ g L^{-1}), the foils were dried in air. The samples were carbon coated prior to the scanning electron microscopy (SEM) measurement with a Polaron CC 7650 SEM (Quorum, UK) for 5×8 s at 2 kV. The diameter of the particles was estimated from the SEM images as an average for >150 particles for each sample.

Photon correlation spectroscopy

A Coulter N4 Plus photon correlation spectroscopy (PCS) spectrometer (Beckman Coulter, USA) with a 10-mW He–Ne laser (632.8 nm) was used. Material **M0** was suspended in water or ethanol, while ethanol or dichloromethane (both Uvasol grade, Merck, Germany) was used for the suspension of modified

particles (materials **M3**, **M4**). The solvents were taken without further purification except nanofiltration (porosity 200 nm, Millipore, France). The values of the viscosities and refractive indices for data evaluation were taken from NIST data compilations [47]. The PCS experiments were performed in quartz cuvettes (d = 1 cm) with suspensions in the concentration range 0.01–1 g L^{-1} at an angle of 90 degrees. The applied concentration was varied to keep the intensities of the detector signal in an appropriate range ($5 \times 10^4 - 2 \times 10^6$ s^{-1}). All experiments were performed at 20 °C using temperature equilibration for 5 min before each run. The data are the result of 10 independent scans and three different samples for each material. The scan time was 5 min. The data were recorded on a standard Pentium PC with the commercial N4 Plus software (Beckman Coulter) and deconvoluted using a size distribution processor based on the Contin algorithm [48, 49], providing an analysis of sizes ("31 pins analysis").

Cyclic voltammetry

Cyclic voltammograms were recorded with a BAS 100 B/W electrochemical workstation (control program version 2.0; Bioanalytical Systems, USA). All electrochemical experiments were carried out at room temperature under argon with a gastight, full-glass, three-electrode cell. The working electrode was a Pt disk electrode (Metrohm, Germany, electroactive area $A = 0.064$ cm^2). The disk was polished before each experiment with α-Al_2O_3 (0.05 μm; Buehler, USA). The counter electrode was a platinum wire (diameter 1 mm) spiral with an outer diameter of 7 mm. As potential reference, a Haber–Luggin double-reference electrode [50] was used. The resulting potentials refer to the Ag/Ag^+ redox system (0.01 M in CH_3CN with 0.1 M NBu_4PF_6). All potentials in this paper are reported to an external fc/fc^+ standard [51] and were rescaled to $E^0(fc/fc^+) = +0.218$ V (dichloromethane) or +0.095 V (acetonitrile) vs. Ag/Ag^+.

Electrochemical quartz crystal nanobalance gravimetry

An EQCN-701 system with a potentiostat PS-305 (both Elchema, USA) was used for EQCN/CV experiments in a three-electrode set-up with an Elchema Ag/AgCl reference electrode, a Pt-sputtered 5-MHz AT-cut quartz crystal without any adhesive layer (ICM, USA) and a Pt spiral wire (d = 1 mm). The crystals were glued to the vertical side of an Elchema cell (V = 30 ml) with 3140 RTV coating silicon (Dow Corning, USA). The experiment was controlled by a sweep generator (EG&G, USA) and connected to a PC via a built-in A/D converter. The data were collected with the LabView software (National Instruments, USA) and subsequently processed with Origin 6.0. Before each experiment, the crystal was rinsed with H_2SO_4/HNO_3 (1:1, v/v), water, and acetone. Its electrochemically active area was estimated from fc measurements. The mass/frequency calibration of the crystal was performed according to a procedure described by Halseid [52].

Other physicochemical methods

Magic-angle spinning (MAS) phosphorus-31 variable-amplitude cross-polarisation (VACP) NMR spectra of powder samples were acquired in 4 mm o.d. zirconia rotors at 10 kHz spinning frequency using Bruker double-bearing MAS probes. Samples were measured on a Bruker AVANCE DSX-200 spectrometer (B_0 = 4.7 T) with 4.2 μs proton pulse widths and contact times of 2 ms, using a ramped-amplitude (2 dB) on the phosphorus channel. Chemical shifts were referenced with respect to external 85% aq. H_3PO_4 by setting the peak of external $NH_4H_2PO_4$ to 0.81 ppm.

The ^1H, $^{13}C\{^1H\}$, $^{31}P\{^1H\}$, and $^{29}Si\{^1H\}$ solution or suspension nuclear magnetic resonance spectra (NMR) were recorded on a Bruker DRX 250 or a Bruker DRX 400 spectrometer at 295 K. Frequencies and standards are as follows: $^{31}P\{^1H\}$ NMR (101.26 MHz), the signals were referenced to external 85% H_3PO_4, ^1H NMR (250.13 MHz and 400.13 MHz), $^{13}C\{^1H\}$ NMR (62.90 MHz), and $^{29}Si\{^1H\}$ (250.13 MHz). The chemical shifts were measured relative to solvent peaks, which are reported relative to TMS. The assignments were supported by two-dimensional COSY, as well as DEPT 135 experiments.

IR, DRIFT, and MS were performed as standard routine measurements. For BET experiments, we used an ASAP 2000 instrument (Micrometrics, USA) determining N_2 isotherms at 77 K (Center for Applied Geosciences, Universität Tübingen).

Syntheses

Synthesis of bare Stöber silica particles (**M0**), based on [21]

Aqueous ammonia ($\rho = 0.900$ g cm^{-3}; 45.2 ml), isopropanol (800 ml; Fluka), and deionized water (55.8 ml) were mixed and heated under stirring in a cap vial until a temperature of 40°C was reached (approximately 1 h). Then, tetraethoxysilane (TEOS; 120 ml, Merck) was added, and the mixture was stirred for 1 h.

Subsequently, the milk-like solution was centrifuged at 4,000 rpm for 3 min, leading to the separation of the particles. The sediment was washed twice with water and twice with isopropanol using ultrasonication and centrifugation after each step, and dried subsequently.

A sample of the silica particles was then checked by optical microscopy (Hertel & Reuss 100:1 oil, numerical aperture 1.3) and SEM. Impurities on or within the particles were controlled by solid-state CP/MAS-NMR. The silica particles were heated in a tube oven under atmospheric conditions to 600°C for 4 days. After cooling down, the product was washed twice with water, twice with isopropanol, twice with hydrochloric acid (10%), and finally three times with water. The yield was 14.4 g (45 %). Upscaling of the reaction up to 5 l was possible without problems by using mechanical stirrers made of PE.

The final shape was controlled by SEM. Amorphousness of the particles was proven by powder X-ray diffraction (Stoe STADI-P, $\theta/2\theta$-geometry, Cu-K_α radiation, Ge monochromator).

Reagents for surface modification

3-(Aminopropyl)-triethoxysilane, 3-(2-aminoethylamino)-propyl-trimethoxysilane (both ABCR, Germany), ferrocenecarboxylic acid **4** (Aldrich), and N-(3-dimethylaminopropyl)-N′-ethylcarbodiimide hydrochloride (Fluka) were used as received.

N-[(3-triethoxysilyl)-propyl]ferrocenecarboxamide 3[1] Ferrocenecarboxylic acid **4** (460 mg, 2 mmol) and N-(3-dimethylaminopropyl)-N′-ethylcarbodiimide hydrochloride (420 mg, 2.2 mmol) were suspended in 20 ml of dichloromethane by sonication. 3-(Triethoxysilyl)-propylamine (800 µL, 2.46 mmol) was added and the solution was stirred for 4 h at room temperature. The clear brown solution was concentrated to 4 ml and separated by column chromatography with silica gel as the stationary phase and a mixture of dichloromethane and acetone 1/8 as the eluent. After removal of the solvent in vacuo, an orange solid was obtained; yield: 323 mg (37%). The spectroscopic data for **3** are given in [53].

Complex 5 was prepared according to [54].

Complex 6 Complex **5** (203 mg, 307 µmol) was dissolved in 10 ml of dichloromethane. A solution of [3-(2-aminoethylamino)propyl]trimethoxysilane (160 µl, 724 µmol) **2** in 5 ml of dichloromethane was added dropwise. The mixture was stirred for 2 h at room temperature and then concentrated to 4 ml in vacuo. The suspension formed after addition of 25 ml of pentane was stirred for 30 min and then filtrated. The solid product was washed five times with pentane, resulting in the yellow product **6** (yield: 203 mg, 75%). $^{31}P\{^1H\}$NMR ($CDCl_3$): δ 35.6 (d,$^2J_{PP} = 36.45$ Hz), 38.9 (d,$^2J_{PP} = 36.45$ Hz). ^{1}H-NMR ($CDCl_3$): δ 0.0 (2H, m, $SiCH_2$), 1.3 (2H, m, $SiCH_2C\underline{H}_2$), 2.3–3.1 (20H, m, $NHC\underline{H}_2CH_2NH_2$, $NHCH_2C\underline{H}_2NH_2$, $PC\underline{H}_2$, $PCH_2C\underline{H}_2$, $CH_2OC\underline{H}_3$, $SiCH_2CH_2C\underline{H}_2$), 3.48 (9H, s, $SiOC\underline{H}_3$), 5.24 (1H, s, $CH_2N\underline{H}$), 7.17–7.73 (20H, m, C_6H_5). $^{13}C\{^1H\}$NMR ($CDCl_3$): δ 6.4 ($Si\underline{C}H_2$), 21.6 ($SiCH_2\underline{C}H_2$), 24.6, and 26.6 (d, $^1J_{PC} = 26.95$ Hz, $P\underline{C}H_2$), 42.5 ($NHCH_2\underline{C}H_2NH_2$), 48.9 ($NH\underline{C}H_2CH_2NH_2$), 50.3 ($Si(O\underline{C}H_3)$), 54.1 ($SiCH_2CH_2\underline{C}H_2$), 57.4, 57.6 (2s, OCH_3), 68.8–69.1 (m, $\underline{C}H_2OCH_3$), 127.6, 127.7, 128,0, 128.3 (4d, $^3J_{PC} = 8.76$ Hz, *m*-C_6H_5), 128.7, 129.0 (2s, *p*-C_6H_5), 131.5, 132.01 (2d, $^2J_{PC} = 8.1$ Hz, *o*-C_6H_5), 132.00, 133.36 (2d, $^1J_{PC} = 36.38$ Hz, *ipso*-C_6H_5), 133.37 (m, *o*-C_6H_5), 134.2 (d, $^1J_{PC} = 32.34$ Hz, *ipso*-C_6H_5), 136.5 (d, $^1J_{PC} = 28.97$ Hz, *ipso*-C_6H_5). IR (in KBr): υ/cm^{-1} 3264–3346 (NH, NH_2), 3053 (aromatic CH), 2935 (aliphatic CH), 1433 (CH), 1191 (C-O), 1087 (Si-O). MS(FAB): m/z: 884.2 (M^+), 847 (M - Cl), 660.1 (M^+ - diamine ligand), 393.9 (M - 2 etherphosphine ligands), 245 (etherphosphine ligand).

Surface modification of particles

3-Aminopropyl-modified silica (M1) After activation at 200°C for 4 h in vacuo, **M0** (2 g; approximately 60 µmol silanol groups on the particle surface as determined from the BET surface and the silanol surface concentration given in [25], see "Results and discussion") was suspended by sonication in 15 ml of anhydrous toluene. 3-(Aminopropyl)-triethoxysilane (40 µl, 123 µmol) was added and the suspension was heated to reflux under argon for 20 h. The modified particles were separated from the solution by centrifugation and washed twice with toluene and twice with freshly distilled *n*-hexane. After drying, the product showed a positive result for the Kaiser test [55].

3-(2-Aminoethylamino)-propyl-modified silica (M2) After activation at 200 °C for 4 h in vacuo, **M0** (2 g; approximately 60 µmol silanol groups on the particle surface) was suspended by sonication in 15 ml of anhydrous toluene. Then, [3-(2-aminoethylamino)propyl]trimethoxysilane (32 µl, 144 µmol) was added and the suspension was heated

[1]The procedure for preparation of **3** has been described previously in [53]. Inadvertently, an essential part of the procedure was omitted, and therefore, full details are given here.

to reflux under argon for 20 h. The particles were separated from the solution by centrifugation and washed twice with toluene and twice with freshly distilled *n*-hexane. After drying, the product showed a positive result for the Kaiser test. ^{1}H-NMR (in $CDCl_3$ suspension): δ 0.8 ($SiCH_2CH_2CH_2$), 1.3 ($SiCH_2CH_2CH_2$), 3–4.5 (broad, NH, NH_2, CH_2).

Ferrocenecarboxamide-modified silica (M3) via route I Ferrocenecarboxylic acid **4** (21 mg, 86 μmol) and *N*-(3-dimethylaminopropyl)-*N*′-ethylcarbodiimide hydrochloride (19 mg, 100 μmol) were dissolved in 10 ml of toluene. **M1** (1 g) was added and the suspension was stirred for 72 h. The particles were then separated by centrifugation and washed twice with toluene and five times with dichloromethane. The Kaiser test generates only a slightly blue color.

Ferrocenecarboxamide-modified silica (M3) via route II After activation at 200 °C for 4 h in vacuo, **M0** (2 g; approximately 60 μmol silanol groups on the particle surface) was suspended by sonication in 20 ml of anhydrous toluene. Then, a solution of **3** (80 mg, 180 μmol) in 5 ml of toluene was added and the suspension was heated to reflux under argon for 20 h. The particles were separated from the solution by centrifugation and washed twice with toluene and five times with dichloromethane. ^{13}C-CP/MAS-NMR: δ 7.9 (Si-CH_2), 21.9 (Si-CH_2-CH_2), 43.4 (Si-CH_2-CH_2-CH_2), 69.8 ($C_{10}H_9Fe$), 171 (weak, C=O).

(Diamine)(diphosphine)(dichloro)-ruthenium(II)-modified silica (M4) via route I **M2** (1 g) was suspended in 15 ml of toluene by sonication. Complex **5** (50 mg, 76 μmol) was added to the suspension and stirred at 40 °C overnight. The particles were then separated by centrifugation and washed four times with toluene and three times with *n*-hexane. After drying, the product did not show a color change for the Kaiser test. ^{31}P-VACP/MAS-NMR: δ 20–60 (br); ^{1}H-NMR (in $CDCl_3$ suspension): δ 0.9 ($SiCH_2CH_2CH_2$), 1.3 ($SiCH_2CH_2CH_2$), 3–5 (broad, NH, NH_2, CH_2, CH_3), 7.3–7.9 (aromatic protons).

(Diamine)(diphosphine)(dichloro)-ruthenium(II)-modified silica (M4) via route II After activation at 200 °C for 4 h in vacuo, **M0** (2 g; approximately 60 μmol silanol groups on the particle surface) was suspended by sonication in 20 ml of anhydrous dichloromethane. Then, a solution of **6** (180 mg, 272 μmol) in 10 ml of dichloromethane was added and the suspension was stirred at room temperature for several days under argon. The particles were then separated from the solution by centrifugation and washed several times with acetone. The ^{1}H-NMR spectrum in $CDCl_3$ suspension is essentially identical to that of **M4** via route I.

Results and discussion

Bare Stöber silica particles, material **M0**

The process of Stöber silica nanoparticle formation is based on the partial hydrolysis of tetraalkoxysilanes in alcoholic media catalyzed by ammonia:

$$Si(OR)_4 + H_2O \leftrightarrows (OR)_3Si(OH) + ROH \qquad pH = 7 \tag{1}$$

followed by a condensation

$$(OR)_3Si(OH) + H_2O \leftrightarrows SiO_2 + 3ROH \tag{2}$$

Various parameters (e.g., temperature, stirring rate, addition rate of TEOS, ammonia concentration) influence the quality of the resulting particles [56]. In particular, strong stirring is necessary to avoid agglomeration. SEM images (Fig. 1) prove that careful control of the reaction conditions reproducibly yields monodisperse and spherical silica particles. Optical microscopy provides an estimate of their diameter, $d \approx 0.8$ μm in the present case.

As demonstrated by solid state ^{13}C CP/MAS-NMR, the silica material contains significant amounts of isopropanol after initial isolation, despite intensive washing ("Experimental section"). Possibly, the alcohol is incorporated into the particles during the sol-gel process. Further weak NMR peaks can be assigned to

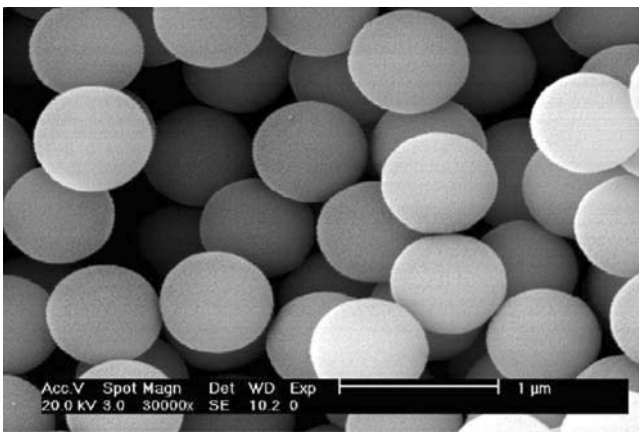

Fig. 1 SEM image of gold sputtered material **M0**

included ethanol, which is the result of TEOS hydrolysis. The isopropanol and ethanol content makes the raw material unsuitable as the basis for organic surface modification. However, heating to 600 °C appears to evaporate and pyrolyze all incorporated organic material. Organic contaminations in the particles were absent after this calcination procedure. No changes of the particle geometry by heating were detected by SEM. Powder X-ray diffraction of the silica particles before and after calcination did not indicate any phase conversion from amorphous to crystalline SiO_2. It is known, however, that calcination at the temperature indicated leads to condensation of silanol groups inside and on the surface of the particles [25]. Consequently, the molecular structure of the particles becomes more dense. Some remaining isolated silanol groups in our material could be detected by ^{1}H-NMR and DRIFT spectroscopy. After additional treatment with hydrochloric acid, the surface of the particles becomes rehydroxylated [25].

Ruthenium(II) complex **6**

The conjugate of **5** and 3-(2-aminoethylamino)-propyl-trimethoxysilane (**6**, Scheme 2) was isolated prior to immobilization on silica and characterized. Results of the structural analysis provided by ^{1}H- and ^{13}C-NMR spectroscopy are fully compatible with the spectra obtained from a (diamine)(dichloro)(diphosphine)ruthenium(II) complex with an unsymmetrical diamine ligand [32]. Moreover, the ^{31}P{^{1}H}NMR spectrum displays an AB pattern (δ 38.9, 35.6, $^2J_{PP}$ = 36.45 Hz) due to the two inequivalent phosphine groups, which compares well (δ 39.1, 38.9, $^2J_{PP}$ = 36.7 Hz) with reference compounds [32].

A cyclic voltammetric study in CH_2Cl_2 revealed an almost uncomplicated diffusion-controlled one-electron oxidation process without follow-up reactions at $E^0 = -0.062 \pm 0.003$ V. The peak potential difference in the voltammograms indicates a high electrochemical reversibility (fast electron transfer) similar to other ruthenium(II) complexes with the $N_2P_2Cl_2$ ligand set [27]. From the peak currents in the diffusion-controlled experiments with dissolved **6**, a diffusion coefficient $D = 1.2 \pm 0.2 \times 10^{-5}$ cm^{2}s^{-1} was determined.

A deviation of the i_p vs $v^{1/2}$ plot from linearity was apparent only at slow scan rates ($v = 0.02$ V s^{-1}). This may be assigned to a very slow adsorption process of **6** on the Pt electrode surface. Indeed, exposing a clean Pt electrode to a solution of **6** overnight resulted in a visible precipitate on the surface. The electrode thus modified could be transferred into an electrolyte without redox-active compound and exhibited a redox signal of a surface-confined species ($i_p \sim v$).

Surface modification of particles

Aminoalkyl-modified silica particles, materials **M1** *and* **M2**

The modification procedures used in this work rely on the reactivity of the hydroxyl functions on the Stöber silica particle surface [57, 58]. The successful immobilization of aminoalkylsilanes on **M0** to form **M1** or **M2** is proven by the results of Kaiser tests [55]. A deep blue color appears in suspensions of **M1** and **M2**, indicating the presence of primary amino groups bound to the silica materials. **M1** and **M2** were also characterized by NMR techniques. For solid-state NMR experiments, the amount of the modifiers on silica was too low to lead to reasonable signal-to-noise ratios. However, suspension ^{1}H-NMR experiments provided significantly better results for **M2**, and the signals can be assigned by comparison to those observed for the 3-(2-aminoethylamino)-propyl-trimethoxysilane modification reagent.

We conclude that the aminoalkyl modifiers are present on the surface of **M1** and **M2** and are possibly bound covalently to the particles, which allows us to use these materials for further modification.

Ferrocenecarboxamide-modified silica particles, material **M3**

Materials **M3** from routes I and II were characterized by solid-state ^{13}C-CP/MAS-NMR. The results were compared to ^{13}C-NMR spectra of ferrocene derivative **3** in order to prove immobilization of the fc species. **M3** prepared via route I by the reaction of **M1** with ferrocene carboxylic acid **4** shows only weak signals, tentatively assigned in analogy to **3** [53], indicating a low surface concentration of the modifier on the silica particles. Indeed, according to the Kaiser test, the amount of residual –NH_2 moieties is rather high, even if the reaction time of **M1** and **4** was extended to 72 h. Consequently, the reaction seems to proceed with only low yield.

In contrast, the reaction of **M0** with **3** (route II) provided significantly higher yields of the immobilized ferrocene species according to solid-state ^{13}C-CP/MAS-NMR spectra. The NMR spectra correlate well with those of **3**. The absence of signals of the ethoxy groups originally present in **3** suggests the successful covalent immobilization and proves that Si–O–Si bonds are formed between **3** and the silica surface.

(Diamine)(diphosphine)-ruthenium(II)-modified silica particles, material **M4**

Similar to material **M3**, **M4** can be prepared by both synthetic routes I and II, based on the reaction of the hemilabile etherphosphine ruthenium(II) complex fragment in **5** with **M2** or conjugate **6** with **M0**. The common diamine component in the former reaction was already replaced [26] by a diamino-trialkoxysilane immobilized on a Pt-surface leading to structurally very similar species, as obtained in the corresponding homogeneous reaction [31]. Thus, the immobilized diaminosiloxane linker is acting as a bidentate ligand. Its reaction leads to a substitution product [26].

In the ^{31}P-VACP/MAS NMR spectrum of **M4**, broad resonances in the range of 20 to 60 ppm indicate that the metal complex has been immobilized successfully to the silica particles. This broad chemical shift range seems to be in contrast to the rather small chemical shift difference of the P atoms in complex **6**. Going from solution to materials like **M4**, however, generally, line widths of the signals increase and fine structure is lost due to increasing dispersion of the chemical shifts. Previous results on comparable (diamine)(dichloro)(diphosphine)ruthenium complexes demonstrate isomerization to all-*cis*-$RuP_2N_2Cl_2$ or *cis-cis-trans*-$RuP_2N_2Cl_2$ structures when changing from solution to the solid state [28, 29, 31, 32, 59]. Moreover, a detailed single-crystal diffraction analysis and a comprehensive ^{31}P solid state NMR investigation showed that, already, a simple (diamine)(diphosphine)ruthenium complex can have a complicated crystal structure and a broad range of ^{31}P chemical shifts [59]. Complex **6** may form isomers with slight structural differences on the silica particles. Thus, the broad range of chemical shifts in the ^{31}P-VACP/MAS NMR spectra of **M4** is fully compatible with the (diamine)(diphosphine)ruthenium complex moiety.

Direct attachment of species **6** (Scheme 2, route II) on silica **M0**, however, did not lead to satisfactory yields. Although weak signals from suspension ^{1}H NMR experiments suggest the presence of the immobilized ruthenium(II) complex, the intensities and the very weak solid-state ^{31}P NMR signal indicate a low surface concentration of the complex.

Comparison of synthetic routes to **M3** *and* **M4**

For the two types of modifiers used, two different synthetic routes proved to be successful: route II for the ferrocene and route I for the ruthenium complex moiety. In the ferrocene case, the reactive intermediate for the amide bond formation in route I is the anhydride of ferrocene carboxylic acid [53]. Possibly, this anhydride reacts with adsorbed water on the silica surface and the immobilized amine competitively, thus reducing the amide yield. Such a side reaction is not expected for route II. Material **M3** synthesized via route II with a higher surface concentration of modifier was subsequently used for the further electrochemical investigations presented in this paper.

The low yield of surface modification by route I in the ruthenium complex case is a consequence of the hindered reaction between the triethoxy groups of **6** and the hydroxyl groups of silica **M0** at room temperature. On the other hand, complex **6** is thermally labile at elevated temperatures. Such conditions could, thus, not be employed. However, this problem is overcome by route II, where the aminosiloxane is immobilized at higher temperature prior to ligand substitution. Therefore, **M4** obtained by the latter procedure represents the material further used in this work.

Size estimation

The geometrical properties of the particles that constitute materials **M0**–**M4** were characterized by means of PCS (in suspension; Table 1) and SEM (in vacuum; Fig. 1 and Table 1). Besides providing quantitative information about the monodispersity of the materials, the PCS technique allows to characterize the behavior of the particles in suspension. Slight changes of solvent properties (polarity, pH, ionic strength) can play a crucial role for the colloidal character of the particles [60, 61]. Consequently, the diameter and the size distribution in different solvents provide essential information for their further uses, e.g., their surface modification or interaction with an electrode surface. Thus, the PCS measurements of all materials were

Table 1 Properties of synthesized silica materials

Parameter	M0	M3	M4
d_{PCS}/nm	755[a]/763[b]	763 [c]	768[c]
d_{SEM}/nm	735 ± 23	748 ± 37	751 ± 26
E^0/V		0.152 ± 0.009	−0.040 ± 0.003
ΔE^0 [d]/V		−0.023	−0.007

[a]In water
[b]In ethanol
[c]In dichloromethane
[d]Shift of the formal redox potentials as compared to the freely diffusing species (**4** or bis(η^1-methoxyethyldiphenylphosphine)(ethylenediamine)dichlororuthenium(II) [26], respectively)

carried out in water, ethanol, and dichloromethane. In contrast, the SEM experiments characterize the particles in vacuum without such complications.

The PCS characterization of **M0** revealed significant differences in the size distribution in the solvents mentioned (Fig. 2a–c). While the measurements in polar solvents (water, ethanol; Fig. 2a and b) showed a single maximum of the particles' size distribution close to 800 nm, the distribution in dichloromethane exhibited several maxima spread up to 3,000 nm at multiples of the expected particle diameter (Fig. 2c). The maxima represent most likely agglomerates in suspension composed from two or more silica particles. We assume that the monodispersity of the particles' suspension in water and ethanol is a consequence of electrostatic interactions, which predominate in polar media [62]. Most probably, the interaction of the hydrophilic particle surface with polar protic solvent molecules stabilizes the high surface energy. This leads to a large number of single particles in the suspension. Therefore, a single maximum is exhibited in the PCS data. In less polar and aprotic solvents like dichloromethane, on the other hand, such stabilizing effects are absent, and the particles tend to decrease their overall surface by agglomeration. Similar results in terms of agglomeration were observed for the amino-modified materials **M1** and **M2** (Fig. 2d–g).

In contrast, the redox-actively modified materials **M3** and **M4** showed a reverse behavior. Agglomerates of **M3** and **M4** particles are formed preferably in polar

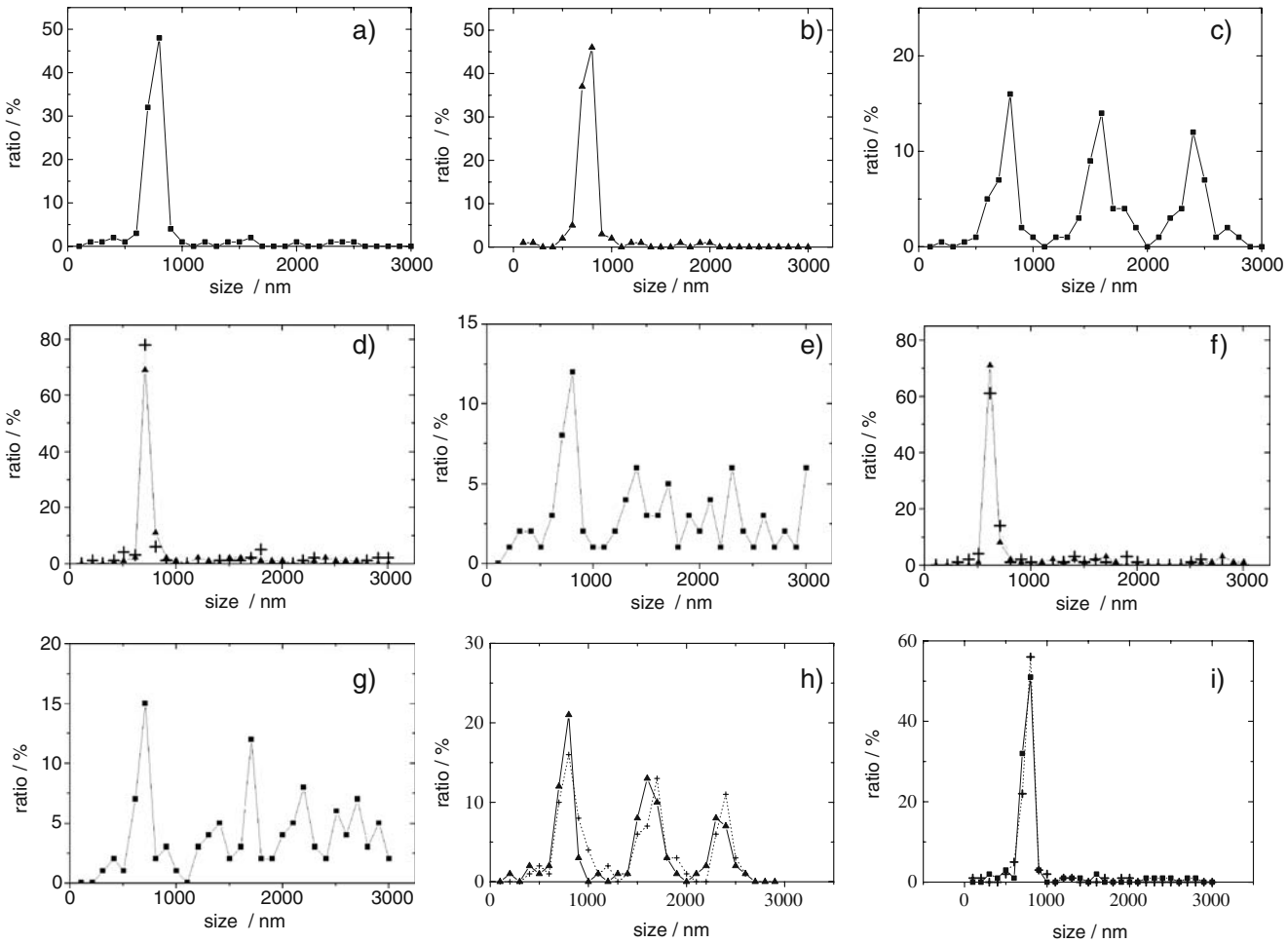

Fig. 2 Size distribution of **M0** (**a**–**c**) and modified Stöber silica particles (**M1**–**M4**) determined by PCS in different solvents; **a** **M0**/water, **b** **M0**/ethanol, **c** **M0**/dichloromethane, **d** **M1**/water (*triangles*) and ethanol (*crosses*), **e** **M1**/dichloromethane, **f** **M2**/water (*triangles*) and ethanol (*crosses*), **g** **M2**/dichloromethane, **h** **M3** (*triangles*) and **M4** (*crosses*)/water, and **i** **M3** (*triangles*) and **M4** (*crosses*)/dichloromethane

solvents such as water (Fig. 2h), while single particles dominate in the dichloromethane suspension (Fig. 2i). Thus, the surface properties of the modifiers determine the stability of the particle suspensions [63]. In our particular case, the hydrophobic groups of fc (cyclopentadienyl rings) and the ruthenium(II) complex (phenyl rings) induce the agglomeration in polar solvents, while an aprotic solvent, such as CH_2Cl_2, does stabilize the individual particles by solvation.

The presence of a single maximum in the size distribution of **M0** in the protic solvents allows us to evaluate the diameter of the particles (Table 1). The result correlates well with values obtained from the SEM experiments. It has to be noted that the determination of a standard deviation for d from the PCS experiments was hampered by low reproducibility. The diameters of **M3** and **M4** were estimated from the maximum of the PCS data in the monodisperse dichloromethane suspensions (Table 1) and compared with the values obtained from SEM. The diameter estimated from both SEM and PCS is very close to that found for **M0**. Moreover, the particle diameter is almost identical for all materials. This is expected for the hard spherical support in the present cases, which is covered by a thin molecular modifying layer. In the following, the SEM diameter is used for further interpretations.

Surface area and porosity

The porosity of particles **M0** was determined by BET measurements. The adsorption branch of the nitrogen isotherm is characteristic of a material with a specific surface area $S = 4.12\ m^2\ g^{-1}$. Mesopores are not indicated. Assuming a strictly monodisperse distribution of solid spheres of diameter d and density ρ, the geometrical specific surface area is calculated from $S_{geom} = 6/(d \times \rho)$. Inserting $d = 748$ nm and $\rho = 2.2\ g \times cm^{-3}$ [64], $S_{geom} = 3.58\ m^2\ g^{-1}$ is obtained. This value is about 15% smaller than S_{BET}. The discrepancy is probably due to an overestimation of ρ in the calculation of S_{geom}. The BET isotherms indicate the presence of small (micro-)pores, which cause a reduced particle density as compared to ideal solid spheres: The desorption branch of the nitrogen isotherm deviates slightly from the adsorption branch. This phenomenon indicates an activated desorption process due to the presence of micropores with openings smaller than 0.5 nm [65]. Such micropores are accessible for nitrogen molecules, but the larger redox modifiers used in this study should clearly be excluded. Therefore, the Stöber particles can, in the following context, be considered as nonporous, and their geometrical surface area is relevant for further calculations.

Characteristics of the adsorption process

Cyclic voltammetry of adsorbed particle layers

The basic electrochemical features of the modified particles **M3** and **M4** were already described [23]. In particular, the redox potentials of the immobilized redox species do not differ to a large extent from those of freely diffusing model compounds. Moreover, particles **M4** are oxidized at only 22 mV less positive potentials as compared to the modifier complex **6**.

The adsorption of **M3** and **M4** on a metallic electrode (Pt) was characterized by a combination of EQCN experiments and CV, which has been widely applied for the investigation of adsorbed layers on Pt surfaces [66–68]. The current through the electrode and the mass changes of the electrode as a function of the applied potential are observed simultaneously. Thus, we follow the formation of the adsorption layer during a voltammetric experiment.

In a first part of the experiment, the electrode was exposed to a particle suspension for several hours. This guarantees spontaneous deposition of a significant amount of particles.

Typical EQCN/CV signals on Pt-sputtered quartz crystals after adsorption of material **M3** are displayed in Fig. 3. Based on our earlier results regarding the CV of redox-modified Stöber particles [23], the scan rate used here corresponds to a time scale where the current through the electrode is limited by a diffusion-like electron hopping process [40–44] along the particle surface.

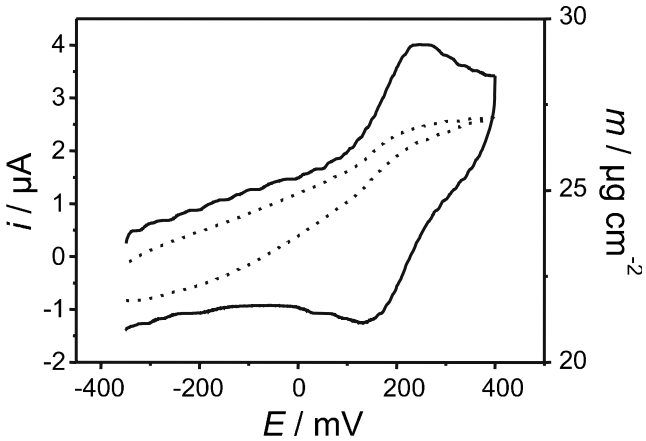

Fig. 3 Voltammetric (*solid line*; not background-corrected) and EQCN (*dotted line*) signals of a Pt-sputtered quartz crystal in a suspension of **M3** ($c = 5.6\ g\ L^{-1}$) after 4 h, $v = 0.02\ V\ s^{-1}$, electroactive area $A = 0.013\ cm^2$, acetonitrile + NBu_4PF_6 (0.1 M) electrolyte at room temperature

An increase of the mass per unit area, m, was detected upon the oxidation of the ferrocene centers at potentials above ≈0.2 V. The mass increase clearly coincides with the onset of the voltammetric current. This increase was followed by a decrease of the detected mass during the reverse (reduction) scan for $E < 0.15$ V. The mass changes during a voltammetric cycle are only about 1% of the mass owing to the spontaneously adsorbed layer of particles (m ≈500 μg cm^{-2}).

The m/E behavior suggests a counter ion and solvent molecule effect observed in a similar way for diaminobutane-ferrocenyl dendrimers [69] and ruthenium(II)(tpy)$_2$ PAMAM dendrimers [70]. Oxidized fc$^+$ immobilized on the particles attached to the electrode attract counter ions (here, PF_6^-) from the electrolyte. Consequently, the detected mass increases upon oxidation, and it decreases on the reverse scan, where the redox centers are reduced and the counter ions are released into the electrolyte.

Spontaneous layer growth

The growth of the adsorbed **M3** and **M4** layers with time are characterized by mass (m) and charge density (σ) variations during the layer growth (Fig. 4). The charge density was evaluated by integration of the voltammetric oxidation wave [71] at $v = 0.02$ V s^{-1}.

The $m = f(t)$ and $\sigma = f(t)$ curves are similar for both particle types. However, the shape of the m and σ dependencies differs. While m rises continuously with time, σ tends to a constant plateau value σ_{pl} (Table 2) after a certain time (t_{pl}). After reaching this point, no further significant changes of σ were detected anymore, although the mass of adsorbed particles continued to increase even until 16 h had passed.

Table 2 Adsorption characteristics from EQCN/CV investigation of **M3** and **M4** adsorbed on a Pt-sputtered quartz crystal; parameters, see Fig. 4, definition of symbols, see text

	M3	M4
t_{pl} / h	4.5	6.5
σ_{pl} / μC cm^{-2}	11.85	8.66
m [a] / μg cm^{-2}	380	420
m [b] / μg cm^{-2}	1,560	1,141

[a] Value of m at σ_{pl}
[b] Value of m after 16 h

If we assume that the Stöber silica particles cannot be deformed and that they are highly monodisperse, a complete monolayer would cover 90.7% [72] of the electrode surface ($A = 0.013$ cm^2 for the **M3** experiments). With a particle radius $r = d/2 = 374$ nm, we estimate $n = 2.68 \times 10^6$ particles in a monolayer, and (with ρ_{SiO_2} as before) the monolayer mass as 1.29 μg (corresponding to 99.2 μg cm^{-2}). Thus, the mass changes observed during spontaneous adsorption experiments indicate the formation of a multilayer. In fact, the mass after 16 h of adsorption indicates an average of 11–15 layers. On the other hand, the coverage when the limiting charge density is reached corresponds to three to four layers attached to the surface. Consequently, only these three or four layers are affected

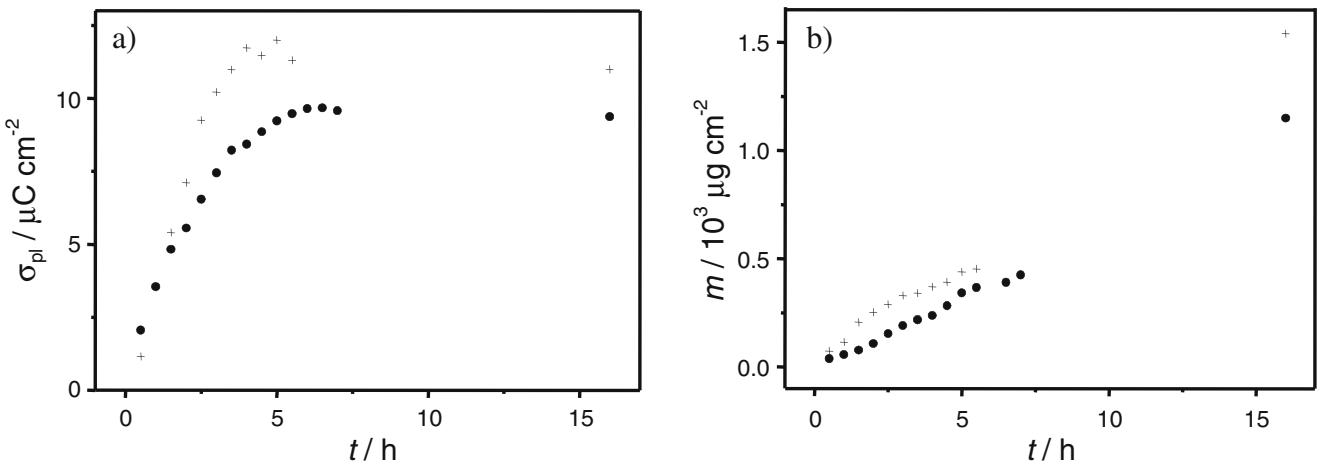

Fig. 4 Growth of the particle layer on a Pt-sputtered quartz crystal in a particle suspension in acetonitrile + NBu_4PF_6 (0.1 M) characterized by charge density σ (**a**) and mass per unit area m (**b**); (*plus signs*) **M3**, $c = 5.6$ g L^{-1}, $A = 0.013$ cm^2; (*circles*) **M4**, $c = 5.4$ g L^{-1}, $A = 0.0105$ cm^2

by the charge transfer. This result shows that redox communication through the multilayer occurs but is limited to about three layers, most probably governed by the extension of the diffusion layer induced by the electron transfer [23].

SEM imaging under conditions identical to those as described for the EQCN/CV experiments were performed with Pt foils exposed to the suspensions for 2 and 4 h. After 2 h (Fig. 5a), **M3** shows the growth of a layer on the Pt surface. Single particles or groups of several spheres preferably form the layer of **M3** in contrast to **M4** (Fig. 5c). In the latter case, cluster formation prevails. Moreover, the images after 4 h (Fig. 5b, d), where the plateau of σ is almost reached, confirm an even higher ratio of clusters in both the **M3** and **M4** layers. In some regions of the denser **M3** layer (Fig. 5b), a regular structure with hexagonal particle arrangement is observed. The SEM images, however, do not show a compact multilayer after 4 h. Hence, the mass change of the crystal determined seems to be, rather, a result of cluster formation than building of well-ordered multilayers on the Pt surface, and the value of 3–4 monolayers determined above is a statistical result. The structure of these layers and/or control of their growth might be interesting in terms of applications of the modified Stöber particles either in sensor development or interphase catalysis [22].

Layer growth under an applied potential

As reported for other ferrocene species [69, 73], the adsorption process of **M3** or **M4** could be governed by application of a potential near the formal potential of the particles (electrodeposition). Based on the results of the electrochemical characterization, electrodeposition of **M3** was performed at $E = 0.22$ V in CH_3CN. Such a potential is ≈ 30 mV more positive than E^0 for **M3**. Voltammetric and EQCN signals after 2 h are displayed in Fig. 6a, b.

The midpoint potential of the voltammetric wave is essentially identical to that of a spontaneously adsorbed **M3** layer (difference in $\overline{E}$: 4 mV). In addition, the EQCN signal presents the same counter ion effect as described above. The mass of **M3** deposited on the crystal (511 μg cm^{-2}) after 2 h of electrodeposition is higher than the mass after 4 h of spontaneous adsorption. This suggests a faster immobilization on the electrode surface by electrodeposition than by spontaneous adsorption.

The decisive influence of the electrode potential can also be seen from two experiments, where the potential was scanned either in the positive direction in order to successively oxidize the electrode surface or in the negative direction in order to reduce it. A starting potential significantly more negative than E^0 was applied

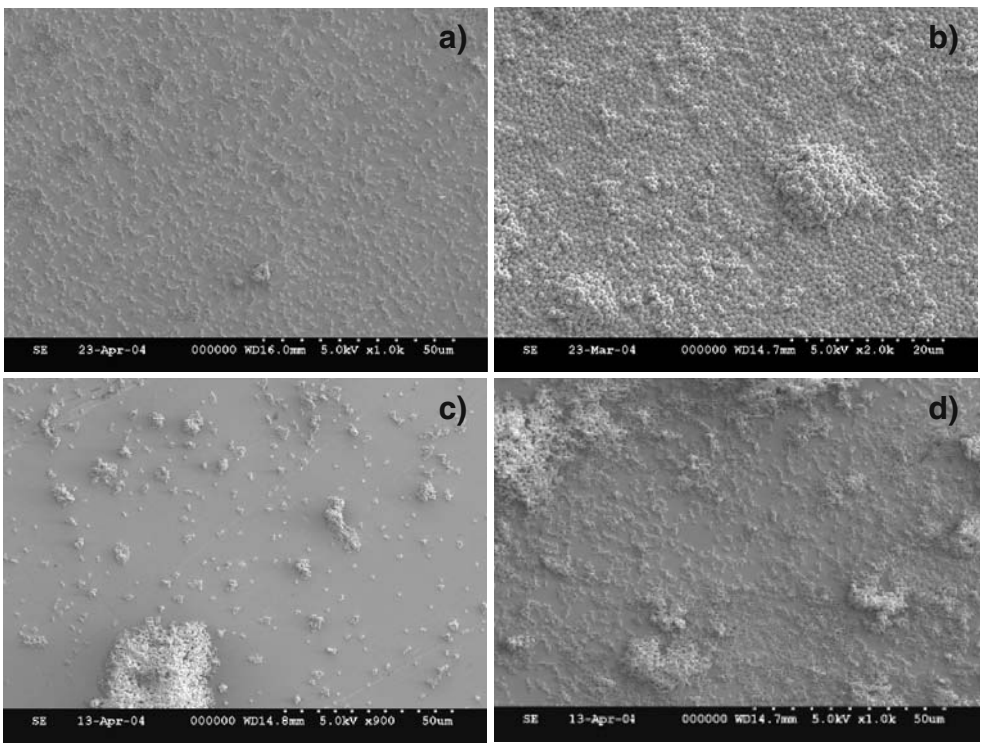

Fig. 5 SEM images of adsorbed particles on a Pt-foil. **M3**: **a** after 2 h; **b** after 4 h; **M4**: **c** after 2 h; **d** after 4 h

for the positive scan (−0.4 V). A potential scan rate of 5 mV min^{-1} enabled to follow the growth of the electrodeposited layer on the crystal. The increase of the mass in such an experiment follows a sigmoidal curve (Fig. 6c). The increase slows down when the potential reaches values positive of E^0. The resulting mass is 20% lower than that observed after 2 h of electrodeposition at a constant potential of 0.22 V but corresponds to that after spontaneous adsorption for 4 h. The applied potential supports the formation of the particle layer on the electrode surface.

The reverse behavior was observed when scanning E in the negative direction. In this case, the electrode surface was covered initially with a particle layer deposited during 2 h at 0.22 V, and then E was scanned starting at 0.6 V (5 mV min^{-1}). A curve with a shape similar to that during the positive-going scan was recorded (Fig. 6d). The difference between the plateau values of the sigmoidal curve (≈ 350 μg cm^{-2}) is almost identical during both experiments. Thus, they are controlled by the same parameters, although in different directions.

However, the final mass during the negative scan does not reach zero but, rather, a constant value even at very negative potentials, indicating a rest coverage of the particles on the electrode. This might be ascribed to particles attached via a Si–O– linkage to the Pt surface, which is a stable covalent bond within a range from −1 to +1 V [74]. Such a linkage is characteristic for siloxanes and was applied in the synthesis of chemically modified electrodes [71]. Indeed, a modification

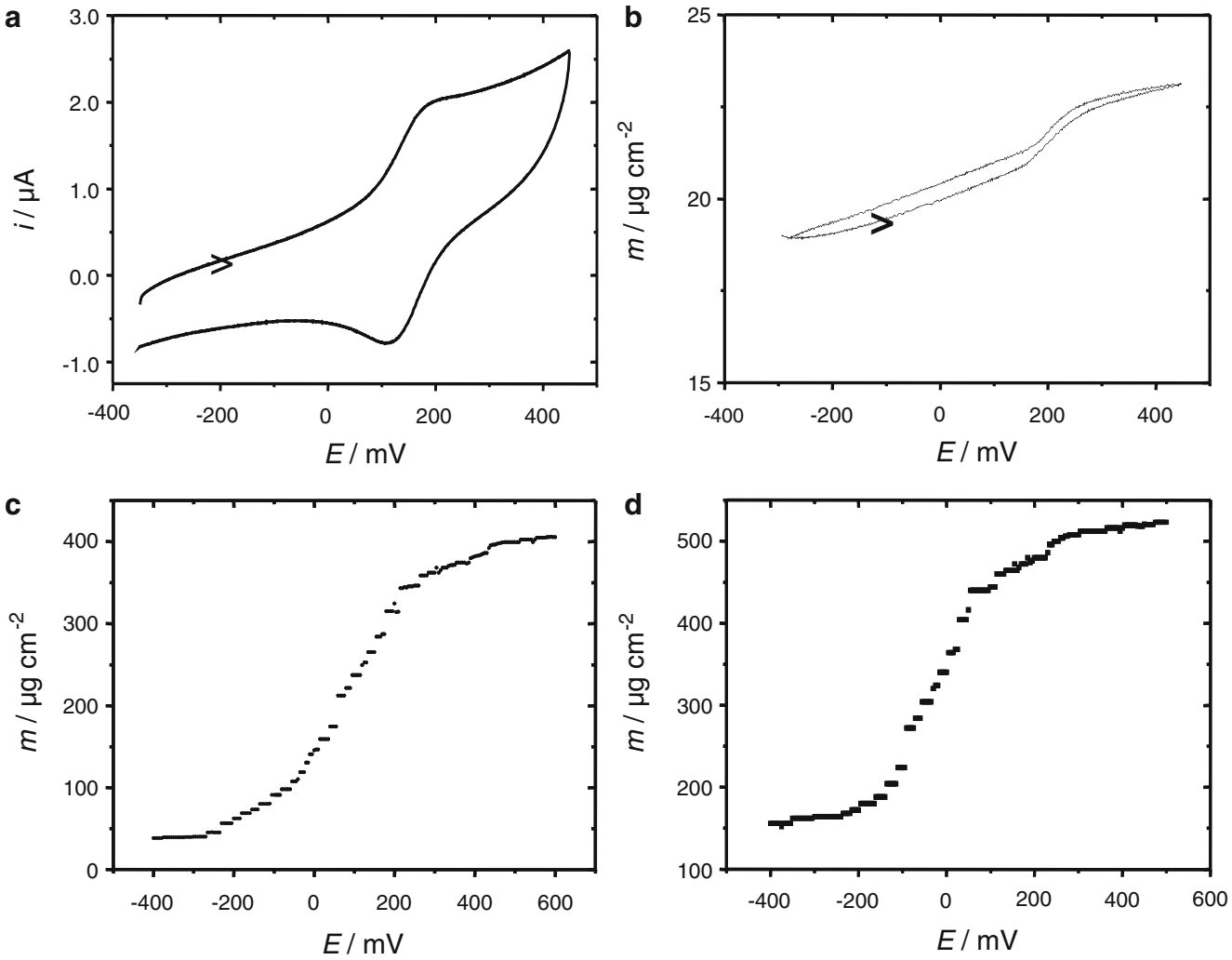

Fig. 6 Electrodeposition of **M3** on a Pt-sputtered quartz crystal ($A = 0.0105$ cm^2). Voltammogram (**a** not background corrected) and corresponding mass signal (**b**) of the quartz crystal exposed to a suspension of **M3** in CH_3CN ($c = 2$ g L^{-1}) at 0.22 V; mass as a function of the potential (scan rate: 5 mV min^{-1}) followed in the positive (**c**) or in the negative direction (**d**)

analogous to the (diamine)(diphosphine) ruthenium complex used in this work was attached to a Pt electrode surface [26].

Conclusions

The controlled synthesis of Stöber silica particles and their further chemical modification by condensation of trialkoxysilanes yields monodisperse, nonmesoporous, spherical silica particles. The optimal modification route is determined by the stability of the particular molecular precursors and the necessary activation of the condensation process.

The modifying layer on the surface of these hybrid materials strongly influences the particle agglomeration behavior. The redox activity of modifying molecules accounts for the particles' electrochemical behavior during adsorption to a metallic electrode and (upon potential variation) in the adsorbed state. These differences might be decisive for a controlled attachment of modified Stöber silica particles to surfaces.

Acknowledgements We thank the Deutsche Forschungsgemeinschaft for support of this work within the Graduiertenkolleg 441 "Chemie in Interphasen," as well as the Max–Buchner–Forschungsstiftung and the Marie Curie training site "SurFace" for providing fellowships to F.N. We acknowledge possibilities to record BET measurements in the Center for Applied Geosciences, Universität Tübingen (Professor Dr. P. Grathwohl, Dr. T. Wendel, and Ms. A. Walz), and SEM pictures in the Institut für Physik, Universität Tübingen (Professor Dr. E. Plies, Ms. Dorothea Adam). We thank Professor Dr. H.-J. Meyer and Ms. Ruth Schmitt (Institut für Anorganische Chemie, Universität Tübingen) for the use of instrumentation and the uncomplicated technical assistance concerning powder X-ray experiments.

References

1. Plumeré N, Speiser B, Mayer HA, Joosten D, Wesemann L (2009) Chem Eur J 15:936–946
2. Willner I, Willner B (2002) Pure Appl Chem 74:1773–1783
3. Astruc D (2003) Pure Appl Chem 75:461–481
4. Rolison DR (2003) Science 299:1698–1701
5. Shenhar R, Rotello VM (2003) Acc Chem Res 36:549–561
6. Schlögl R, Abd Hamid SB (2004) Angew Chem 116:1656–1667 (Angew Chem Int Ed 43:1628–1637)
7. Cushing BL, Kolesnichenko VL, O'Connor CJ (2004) Chem Rev 104:3893–3946
8. Ball P (2004) Nachr Chem 52:131–136
9. Hammond PT (2004) Adv Mater 16:1271–1293
10. Katz E, Willner I (2004) Angew Chem 116:6166–6235 (Angew Chem Int Ed 43:6042–6108)
11. Antonietti M, Ozin GA (2004) Chem Eur J 10:28–41
12. Tomalia DA (2004) Aldrichim Acta 37:39–57
13. Raimondi F, Scherer GG, Kötz R, Wokaun A (2005) Angew Chem 117:2228–2248 (Angew Chem Int Ed 44:2190–2209)
14. Kim JH, Kang M-S, Kim YJ, Won J, Park N-G, Kang YS (2004) Chem Commun 1662–1663
15. Anderson ML, Stroud RM, Rolison DR (2002) Nano Lett 2:235–240
16. Yoon T-J, Kim JS, Kim BG, Yu KN, Cho M-H, Lee J-K (2005) Angew Chem 117:1092–1095 (Angew Chem Int Ed 44:1068–1071)
17. Wallace JM, Rice JK, Pietron JJ, Stroud RM, Long JW, Rolison DR (2003) Nano Lett 3:1463–1467
18. Miller CR, Vogel R, Surawski PPT, Corrie SR, Rühmann A, Trau M (2005) Chem Commun 4783–4785
19. Jang J, Lim B (2003) Angew Chem 115:5758–5761 (Angew Chem Int Ed 42:5600–5603)
20. Unger K, Giesche H, Kinkel J (1987) Kugelförmige SiO_2-Partikel, Patent Ger. Offen. DE 3534143 A1, Merck Patent GmbH
21. Stöber W, Fink A, Bohn E (1968) J Colloid Interface Sci 26:62–69
22. Lindner E, Schneller T, Auer F, Mayer HA (1999) Angew Chem 111:2288–2309 (Angew Chem Int Ed 38:2154–2174)
23. Budny A, Novak F, Plumeré N, Schetter B, Speiser B, Straub D, Mayer HA, Reginek M (2006) Langmuir 22:10605–10611
24. Ling XY, Reinhoudt DN, Huskens J (2006) Langmuir 22:8777–8783
25. Zhuravlev LT (2000) Colloids Surf A 173:1–38
26. Novak F, Speiser B, Lindner E, Lu Z-L, Mayer HA (2004) Angew Chem 116:2059–2062 (Angew Chem Int Ed 43:2025–2028)
27. Lindner E, Lu Z-L, Mayer HA, Speiser B, Tittel C, Warad I (2005) Electrochem Commun 7:1013–1020
28. Lindner E, Warad I, Eichele K, Mayer HA (2003) Inorg Chim Acta 350:49–56
29. Lindner E, Mayer HA, Warad I, Eichele K (2003) J Organomet Chem 665:176–185
30. Lindner E, Ghanem A, Warad I, Eichele K, Mayer HA, Schurig V (2003) Tetrahedron Asymmetry 14:1045–1053
31. Lu Z-L, Eichele K, Warad I, Mayer HA, Lindner E, Jiang Z-j, Schurig V (2003) Z Anorg Allg Chem 629:1308–1315
32. Nachtigal C, Al-Gharabli S, Eichele K, Lindner E, Mayer HA (2002) Organometallics 21:105–112
33. Noyori R (2002) Angew Chem 114:2108–2123 (Angew Chem Int Ed 41:2008–2022)
34. Noyori R, Ohkuma T (2001) Angew Chem 113:40–75 (Angew Chem Int Ed 40:40–73)
35. Merrifield RB (1963) J Am Chem Soc 85:2149–2154
36. Kallury KMR, Macdonald PM, Thompson M (1994) Langmuir 10:492–499
37. Walcarius A, Mandler D, Cox JA, Collinson M, Lev O (2005) J Mater Chem 15:3663–3689
38. Jarzębińska A, Rowiński P, Zawisza I, Bilewicz R, Siegfried L, Kaden T (1999) Anal Chim Acta 396:1–12
39. Anson FC, Ni C-L, Saveant J-M (1985) J Am Chem Soc 107:3442–3450
40. Amatore C, Bouret Y, Maisonhaute E, Goldsmith JI, Abruña HD (2001) Chem Phys Chem 2:130–134
41. Amatore C, Bouret Y, Maisonhaute E, Goldsmith JI, Abruña HD (2001) Chem Eur J 7:2206–2226
42. Takada K, Storrier GD, Goldsmith JI, Abruña HD (2001) J Phys Chem B 105:2404–2411
43. Takada K, Díaz DJ, Abruña HD, Cuadrado I, Gonzalez B, Casado CM, Alonso B, Morán M, Losada J (2001) Chem Eur J 7:1109–1117
44. Goldsmith JI, Takada K, Abruña HD (2002) J Phys Chem B 106:8504–8513

45. Buchmann S, Mayer HA, Speiser B, Seiler M, Bertagnolli H, Steinbrecher S, Plies E (2001) Electrochim Acta 46:3207–3217
46. Dümmling S, Eichhorn E, Schneider S, Speiser B, Würde M (1996) Curr Sep 15:53–56
47. U.S. Secretary of Commerce (2008) http://webbook.nist.gov/chemistry/
48. Provencher SW (1982) Comput Phys Commun 27:213–227
49. Provencher SW (1982) Comput Phys Commun 27:229–242
50. Gollas B, Krauß B, Speiser B, Stahl H (1994) Curr Sep 13:42–44
51. Gritzner G, Kůta J (1984) Pure Appl Chem 56:461–466
52. Halseid R (2004) Ammonia as hydrogen carrier—effects of ammonia on polymer electrolyte membrane fuel cells. PhD thesis, NTNU Trondheim, Norway
53. Schetter B, Speiser B (2004) J Organomet Chem 689:1472–1480
54. Lindner E, Schober U, Fawzi R, Hiller W, Englert U, Wegner P (1987) Chem Ber 120:1621–1628
55. Kaiser E, Colescott RL, Bossinger CD, Cook PI (1970) Anal Biochem 34:595–598
56. Giesche H (2000) In: Sugimoto T (ed), Fine particles, synthesis, characterization, and mechanism of growth, vol 92, Surfactant science series. Dekker, New York, pp 126–146
57. Unger KK (1979) Porous silica. Its properties and use as support in column liquid chromatography, vol 16, J. Chromatogr. Library. Elsevier, Amsterdam, pp 92–96
58. Dorsey JG, Dill KA (1989) Chem Rev 89:331–346
59. Eichele K, Nachtigal C, Jung S, Mayer HA, Lindner E, Ströbele M (2004) Magn Reson Chem 42:807–813
60. Colic M, Fuerstenau DW (1997) Langmuir 13:6644–6649
61. Grübel G, Abernathy DL, Riese DO, Vos WL, Wegdam GH (2000) J Appl Cryst 33:424–427
62. Papirer E, Balard H (1998) In: Legrand AP (ed) The surface properties of silicas. Wiley, Chichester, pp 315–364
63. So J-H, Oh M-H, Lee J-D, Yang S-M (2001) J Chem Eng Jpn 34:262–268
64. Iler RK (1979) The chemistry of silica. Solubility, polymerization, colloid and surface properties, and biochemistry. Wiley, New York
65. Grillet Y, Llewellyn PL (1998) In: Legrand AP (ed) The surface properties of silicas. Wiley, Chichester, pp 23–81
66. Jerkiewicz G, Vatankhah G, Lessard J, Soriaga MP, Park Y-S (2004) Electrochim Acta 49:1451–1459
67. Wright JEI, Cosman NP, Fatih K, Omanovic S, Roscoe SG (2004) J Electroanal Chem 564:185–197
68. Wilson CD, Roscoe SG (2004) Langmuir 20:7547–7556
69. Takada K, Díaz DJ, Abruña HD, Cuadrado I, Casado C, Alonso B, Morán M, Losada J (1997) J Am Chem Soc 119:10763–10773
70. Storrier GD, Takada K, Abruña HD (1999) Langmuir 15:872–884
71. Murray RW (ed) (1992) Molecular design of electrode surfaces, vol 22, Techniques of chemistry. Wiley, New York
72. Müller U (1996) Anorganische Strukturchemie, Teubner, Stuttgart
73. Mine E, Yamada A, Kobayashi Y, Konno M, Liz-Marzán LM (2003) J Colloid Interface Sci 264:385–390
74. Moses PR, Murray RW (1977) J Electroanal Chem 77:393–399